ACS Combinatorial Science

Research Article

pubs.acs.org/acscombsci

Combinatorial Atmospheric Pressure Chemical Vapor Deposition of Graded TiO_2–VO_2 Mixed-Phase Composites and Their Dual Functional Property as Self-Cleaning and Photochromic Window Coatings

Mia Wilkinson,[†] Andreas Kafizas,[‡] Salem M. Bawaked,[§] Abdullah Y. Obaid,[§] Shaeel A. Al-Thabaiti,[§] Sulaiman N. Basahel,[§] Claire J. Carmalt,[†] and Ivan P. Parkin*[,†]

[†]Materials Chemistry Research Centre, Department of Chemistry, University College London, 20 Gordon Street, London, U.K. WC1H 0AJ

[‡]Department of Chemistry, Imperial College London, Exhibition Road, London, U.K. SW7 2AZ

[§]Chemistry Department, King Abdulaziz University, Jeddah, Saudi Arabia 21589

Supporting Information

ABSTRACT: A combinatorial film with a phase gradient from V:TiO_2 (V: Ti ≥ 0.08), through a range of TiO_2–VO_2 composites, to a vanadium-rich composite (V: Ti = 1.81) was grown by combinatorial atmospheric pressure chemical vapor deposition (cAPCVD). The film was grown from the reaction of $TiCl_4$, VCl_4, ethyl acetate (EtAc), and H_2O at 550 °C on glass. The gradient in gas mixtures across the reactor induced compositional film growth, producing a single film with numerous phases and compositions at different positions. Seventeen unique positions distributed evenly along a central horizontal strip were investigated. The physical properties were characterized by wavelength dispersive X-ray (WDX) analysis, X-ray diffraction (XRD), Raman spectroscopy, scanning electron microscopy (SEM), and UV–visible spectroscopy. The functional properties examined included the degree of photoinduced hydrophilicity (PIH), UVC-photocatalysis, and thermochromism. Superhydrophilic contact angles could be achieved at all positions, even within a highly VO_2-rich composite (V: Ti = 1.81). A maximum level of UVC photocatalysis was observed at a position bordering the solubility limit of V:TiO_2 (V: Ti ≈ 0.21) and fragmentation into a mixed-phase composite. Within the mixed-phase TiO_2: VO_2 composition region (V: Ti = 1.09 to 1.81) a decrease in the semiconductor-to-metal transition temperature of VO_2 from 68 to 51 °C was observed.

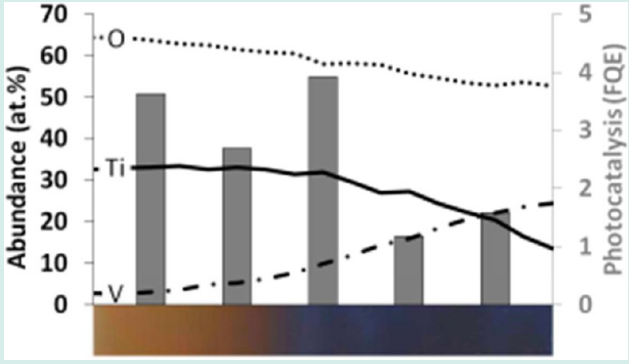

KEYWORDS: *combinatorial, thin-film, TiO_2–VO_2 composite, photocatalysis, photochromism*

I. INTRODUCTION

Titanium dioxide (TiO_2) thin-films have been extensively studied because of their application in a large range of areas, including self-cleaning/water purification,[1,2] water-splitting,[3−5] and gas-sensing.[6] Most research has focused on improving the photocatalytic efficiency to visible/solar light by doping or forming a composite.[7−11] It is the ability of titania to photocatalytically degrade organic waste into carbon dioxide and mineral acids in sunlight and reach a superhydrophilic state, which makes it the material of choice for self-cleaning windows and surfaces.[1] In addition, TiO_2 is nontoxic, chemically stable, inexpensive and stable to extensive photocatalytic cycling—it is a material with great potential to improve water quality though solar driven processes

Vanadium dioxide (VO_2) thin-films find practical use as smart window coatings because of their thermochromic property.[12−20] In the monoclinic form, VO_2 shows a thermally induced and completely reversible semiconductor-to-metal transition (T_C) to the tetragonal (rutile) form at 68 °C. Both electrical and optical properties in the near IR are remarkably affected by the transition, where the monoclinic form behaves as a semiconductor and does not reflect much solar energy and the tetragonal form behaves as a semimetal, reflecting a much wider range of wavelengths.[21] The T_C can be decreased to more moderate temperatures using dopants,[18] which opens up the prospect for being used in architectural glazing that allows heat into a building below the T_C and reflects heat away from a building after the T_C has been surpassed. Such intelligent coatings could reduce the use of internal heating and air-conditioning in a building, leading to savings in energy costs.[13]

Received: February 26, 2013
Revised: May 1, 2013
Published: May 21, 2013

ACS Publications © 2013 American Chemical Society

Thin-films of both TiO_2 and VO_2 can be prepared by a range of methods; the main three technologies being chemical vapor deposition (CVD),[15,22] sol−gel[23,24] and physical vapor deposition (PVD).[25,26] CVD methods have the advantage of being more easily integrated into float-glass production lines.[27] As such, it is the most cost-effective choice for the large-scale coating of glass. It has recently been shown that combining both TiO_2 and VO_2 within a phase composite produces a material that possesses both self-cleaning and thermochromic properties.[28,29] Furthermore, the films showed a 17 °C reduction in the thermochromic switching temperature (T_C = 51 °C). With a further lowering of T_C, these coatings would be strong candidates for self-cleaning solar control glazing.

Combinatorial methods are now widely used in many areas of thin-film science for discovering new materials with unique functions or optimizing existing materials through alloying and doping.[30] Physical vapor deposition (PVD) methods dominate the field as it affords precise compositional control.[31−34] Combinatorial chemical vapor deposition (CVD) methods have been less utilized in this field but possess the advantage of good conformal coverage (even on high aspect-ratio substrates) and cheaper up-scale.[35−50] In traditional CVD, the precursors are combined before entering the reactor. However, combinatorial CVD introduces the precursors into the reactor at separate points. This induces a gradient in gas mixtures across the reactor forcing compositional film growth, resulting in the formation of many phases and compositions across a single film.[39] When the physical and functional properties are characterized in tandem it is possible to find optimum compositions for specific applications.[38] There are two main advantages to the combinatorial approach. First, it can require as little as one synthesis to create a material with a large number of significantly unique states. Second, the large number of unique states formed can be rapidly characterized when high-throughput methods are applied.[51,52]

In this paper we use combinatorial atmospheric pressure CVD (cAPCVD) to synthesize a range of TiO_2−VO_2 composites across a single film. Relationships were drawn between composition and functionality for 17 unique locations across a single strip of film; enabling the quick identification of a section of film with enhanced functional properties. Such analysis of combinatorial thin-films made by the cAPCVD route provides a shortcut to identifying key physical−functional property inter-relationships and offers a faster way of discovering optimum compositions and new materials.

II. MATERIALS AND METHODS

All chemicals were purchased from Sigma-Aldrich Chemical Co; titanium(IV) chloride 99.9%, vanadium(IV) chloride 99.9%, ethyl acetate 99%, stearic acid 99%, and methanol 99%. Nitrogen (oxygen free) gas-cylinders were supplied by BOC. The glass-substrate, consisting of 3.2 mm thick glass coated with a 50 nm SiO_2 barrier layer, was supplied by Pilkington NSG Group. The SiO_2 barrier layer inhibited the migration of ions in the glass. The glass was 89 mm in length and 225 mm in breadth.

Combinatorial Growth of a TiO_2−VO_2 Mixed Phase Composite. Combinatorial atmospheric pressure chemical vapor deposition (cAPCVD) was used to grow a film with transitional phase gradient. The phase varied from V:TiO_2 (V: Ti ≥ 0.08) on one end, through a range of TiO_2−VO_2 composites, to a vanadium-rich composite (V: Ti ≤ 1.81) on the other. The film was grown at 550 °C from the reaction of $TiCl_4$, VCl_4, ethyl acetate (EtAc), and H_2O vapors on glass. A schematic of the cAPCVD apparatus is shown in Figure 1.

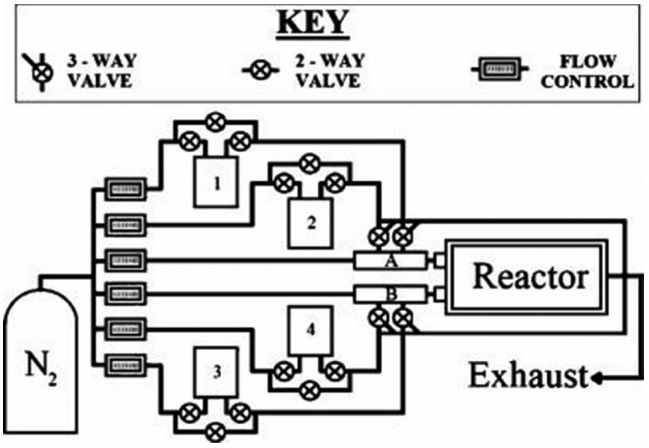

Figure 1. Schematic of the cAPCVD apparatus used in the synthesis of a graded TiO_2−VO_2 mixed-phase composite.

VCl_4 and H_2O were stored in bubblers 1 and 2 respectively. $TiCl_4$ and EtAc were stored in bubblers 3 and 4, respectively. The reagents were volatilized by heating. The vapors that formed were transported with a N_2 carrier gas to their mixing chambers. Vapors of VCl_4 and H_2O were carried to mixing chamber A. Vapors of $TiCl_4$ and EtAc were carried to mixing chamber B. The mixed gases were then carried through a baffle into the reactor. The titanium and vanadium sources were introduced at opposite sides of the reactor. This created a concentration gradient across the reactor and induced a range of deposition conditions required for the combinatorial aspect of the work. The temperature was maintained at 550 °C for the 3 min deposition. The film was cooled under a stream of N_2 to room temperature. The synthetic conditions used to grow the graded TiO_2−VO_2 mixed phase composite are summarized in Table 1.

Table 1. Reaction Conditions in the cAPCVD Synthesis of a Graded TiO_2−VO_2 Mixed-Phase Composite[a]

	mixing chambers		bubblers			
			1	2	3	4
	A	B	VCl_4	H_2O	$TiCl_4$	EtAc
temperature (°C)	160	23	42	60	66	33
flow rate (L min^{-1})	6	6	4	1.5	0.8	0.2
vapor pressure (mm Hg)			20	150	78	136
mass flow (10^{-3} mol min^{-1})			4.5	15.1	3.7	1.8
molar ratios			1.2	4.0	1.0	0.5

[a]Mass flow rate (10^{-3} mol min^{-1}) was calculated from vapor pressure (mm Hg) and flow rate (L min^{-1}).[53] The molar ratio of each reagent is normalized relative to $TiCl_4$.

Physical Characterization of the Combinatorial Film. The film varied in composition most prominently in the horizontal plane (Figure 2a). Thus, positions along a single horizontal plane were analyzed (Figure 2b). The strip analyzed was located at the middle of the film; moving from a TiO_2 rich region on the left to a VO_2 rich region on the right. Positions were spaced 0.5 cm apart.

dx.doi.org/10.1021/co400027p | ACS Comb. Sci. 2013, 15, 309−319

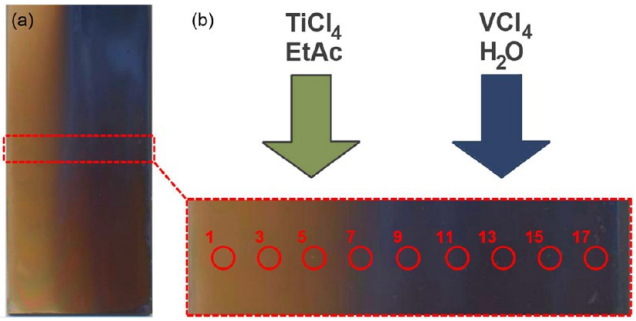

Figure 2. (a) Picture of the entire graded TiO_2−VO_2 mixed-phase composite film formed and (b) a zoomed in image of the midsection, the 17 positions analyzed and the relative point of entry of each precursor.

Each of the 17 grid-positions were analyzed unless stated otherwise. Wavelength dispersive X-ray (WDX) analysis was carried out using a Philips XL30 ESEM, referenced against silicon, titanium, vanadium and oxygen standards. The Ti: V ratio was derived from Ti K_α (4504.9 keV) and V K_α (4944.6 keV) emissions. X-ray diffraction (XRD) mapping was carried out using a microfocus Bruker GADDS powder X-ray diffractometer, with a monochromated Cu K_α (λ = 1.5406 Å) source and a CCD area X-ray detector, capable of 0.01° resolution in 2θ with an automated X-Y movable stage. Raman spectroscopy was conducted with a Renishaw 1000 spectrometer equipped with a 532 nm laser between 100 and 1500 cm^{-1}. The optical reflectance and transmittance spectra were recorded using a Helios double beam instrument over the 200−2500 nm range. The bandgap was derived from Tauc plots of data in transmission.[54] Film thickness was derived by applying the Swanepoel method to data in reflectance.[55] Reflectance spectra of high refractive index materials of uniform thickness display a series of wobbles. The wobbles occur wherever the conditions for constructive and destructive interference of light reflection are met; that is light reflecting from the substrate surface meeting with light reflecting from the film surface. Film thickness can be determined if the spectral dependence of the refractive index is known. As composition and phase changed across the film, an average refractive index value was used for each site analyzed. This average was composed from the refractive index of pure anatase TiO_2 ($n \approx 2.5$)[56] and pure monoclinic VO_2 ($n \approx 2.9$).[57] The weight of each phase was chosen based on the V: Ti ratios determined by WDX analysis. The surface morphology of gold-sputtered samples (Positions 1, 5, 9, 13 and 17) were analyzed by top-down scanning electron microscopy (SEM) using a JEOL-6301F field emission instrument with secondary electron imaging.

Functional Characterization of the Combinatorial Film. *Photoinduced Hydrophilicity.* The degree of photo-induced hydrophilicity (PIH) was related to changes in water droplet contact angle. A 8.6 μL water droplet was cast onto the surface from a shallow height ($\approx$ 1 cm). Samples were initially placed in the dark for 24 h to reset any residual PIH. Contact angles were measured using a First Ten Angstroms 1000 device with a side mounted rapid-fire camera. Each droplet was carefully removed from above the surface utilizing the capillary action of a sponge. Samples were then placed under UVC irradiation (254 nm - Vilber Lourmat 2 × 8W VL-208BLBDH) for a set period of time before the contact angle was remeasured.

Photocatalytic Activity. The photocatalytic activity was measured against the mineralization of a stearic acid overlayer. The overall process for photo-oxidation on a semiconductor photocatalyst corresponds to[11]

$$C_{17}H_{35}COOH + 26O_2 \xrightarrow{\text{air, light} \geq E_{bg}} 18CO_2 + 18H_2O \quad (1)$$

Positions 1, 5, 9, 13, and 17 were assessed. Each sample was first cleaned with acetone and placed under UVC light for 24 h prior to measurement. The stearic acid overlayer was formed by drop-casting a saturated methanolic solution and then drying in an oven at 60 °C for 1 h to evaporate the solvent. The photocatalysis was instigated using UVC light. The degradation of the stearic acid overlayer was monitored by Fourier transform-infrared (FT-IR) spectroscopy using a PerkinElmer RX-I instrument. The level of degradation was quantified by relating the decrease in absorption area of the C−H symmetric and antisymmetric stretches within the 2800−2950 cm^{-1} region to a precalibrated standard.[58] The rate of photocatalysis (molecules degraded cm^{-2} s^{-1}) was determined. The photon flux from the lamp was measured using a UVX-Radiometer equipped with a UVX-25 sensor centered at 254 nm (1.74×10^{15} photons cm^{-2} s^{-1}). The emission profile of the lamp is provided in the Supporting Information, Figure S1. The photocatalytic rate was converted to formal quantum efficiency (FQE) according to the following relationship[11]

$$\text{FQE} = \frac{\text{rate of photocalaysis (molecules degraded}\cdot\text{cm}^{-2}\,\text{s}^{-1})}{\text{incident photon flux (photon}\cdot\text{cm}^{-2}\,\text{s}^{-1})} \quad (2)$$

Photochromism. The thermochromic switching temperature for Positions 13, 15, and 17 (positions located within the VO_2-rich region) was determined by measuring the change in spectral transmittance/reflectance between 200 and 2500 nm with temperature. The spectroscopy was conducted using a Helios double beam instrument. Samples were mounted on a heating stage and heating from 25 to 105 °C in intervals of ≈10 °C. The temperature was measured using a thermocouple mounted directly onto the sample. At each interval the heat was allowed to distribute before the transmittance/reflectance spectrum was measured. The process was repeated when allowing the sample to cool down from 105 to 25 °C. The semiconductor-to-metal transition temperature (T_C) was determined by plotting the change in transmittance/reflectance at 2000 nm; forming a hysteresis loop.[15] Each half of the hysteresis loop was fit to a Boltzmann model using Origin 8.0 software[59] so that the center of the total loop could be accurately identified. The T_C quoted is the average of the two centers identified from studies conducted in transmittance and reflectance, with the error being half the range.

III. RESULTS AND DISCUSSION

Physical Appearance. A graded TiO_2−VO_2 mixed-phase composite was grown by combinatorial atmospheric pressure chemical vapor deposition (cAPCVD). The film was grown on float glass from the combination of $TiCl_4$ and ethyl acetate (EtAc) with VCl_4 and H_2O at 550 °C, coating the entire substrate. On visual inspection the film showed graded color from brown-yellow on the left to a reflective brown-black on

dx.doi.org/10.1021/co400027p | ACS Comb. Sci. 2013, 15, 309−319

Table 2. Summary of the Physical and Functional Properties of the 17 Grid-Positions Analyzed Across a Central Horizontal Strip of a Graded TiO_2–VO_2 Mixed-Phase Composite

	WDX analysis (at. %)					XRD model of crystalline anatase TiO_2 component			Raman	UV–visible spectroscopy			UVC photocatalysis	
	V	Ti	Si	O	V: Ti	a (Å)	c (Å)	volume (Å^3)	E_g ν_6 (cm^{-1})	thickness (nm)	band-gap (eV)	T_C (°C)	molecules degraded (10^{10} cm^{-2} s^{-1})	FQE (10^{-5} molecules photon^{-1})
1	2.7	32.7	0.1	64.5	0.08	3.792	9.553	137.4	149.3	1024	2.52		6.30	3.62
2	2.5	32.9	0.1	64.4	0.08	3.793	9.541	137.2	149.7	1045	2.51			
3	3.1	33.1	0.1	63.7	0.09	3.793	9.539	137.2	150.3	1059	2.49			
4	3.6	33.5	0.1	62.8	0.11	3.793	9.529	137.1	151.4	1062	2.3			
5	4.9	32.6	0.1	62.5	0.15	3.794	9.500	136.7	153.5	1050	2.27		4.69	2.69
6	5.3	33.1	0.1	61.5	0.16	3.793	9.497	136.7	154.8	1033	2.28			
7	6.3	32.7	0.1	60.9	0.19	3.794	9.497	136.7	156.0	994	2.23			
8	7.8	31.6	0.1	60.6	0.25	3.793	9.500	136.7	158.8	918	2.24			
9	9.9	32.0	0.1	58.0	0.31	3.791	9.502	136.6	160.2	828	2.18		6.82	3.92
10	11.9	29.7	0.2	58.2	0.40	3.788	9.471	135.9	159.9	797	1.94			
11	14.5	27.0	0.6	57.9	0.54					629	1.81			
12	15.9	27.3	1.2	55.7	0.58					574	1.59			
13	18.5	24.4	2.3	54.7	0.76					520	1.47	56.2 ± 0.7	2.06	1.18
14	20.6	22.3	3.6	53.5	0.92					480	1.76			
15	22.2	20.4	4.6	52.8	1.09					447	1.77	50.5 ± 4.7		
16	23.7	16.5	6.2	53.7	1.43					394	1.73			
17	24.5	13.6	9.2	52.8	1.81					380	0.69	50.6 ± 1.3	2.76	1.59

the right (Figure 2a). The film varied little in color from top to bottom. This was attributed to the direction of reagent gas flows during the deposition, where the $TiCl_4$ and EtAc sources entered on the left and the VCl_4 and H_2O sources entered on the right. The left side of the film showed colored bands when viewed off angle arising from slight variations in film thickness, which is typical of high refractive index materials such as TiO_2. The colored bands are due to interference patterns from light reflecting from the air-coating and coating-glass interfaces. The brown-yellow color is characteristic of V:TiO_2.[60] The colored bands alternated from green to purple, accumulating in the top-left section of the film. The right side of the film was brown-black and highly reflecting. The alternating colored bands were observed more clearly on the left side of the film, and although present on the right side were less apparent because of the dark and mirror-like nature of the film in this region. The entire film was well adhered, passing the Scotch tape test[61] and stable to submersion in an array of common solvents including methanol, ethanol, and acetone.

Wavelength Dispersive X-ray Analysis. Wavelength dispersive X-ray (WDX) analysis was conducted across all 17 grid-positions (Table 2). A chart showing the Ti, V, Si, and O level (at. %) at each grid-position is shown in Figure 3.

The highest levels of Ti incorporation were observed across grid-positions 1 to 8 (≈ 32–33 at. %). This decreased steadily from grid-position 9 (32.0 at. %) to 17 (13.6 at. %). Conversely, the level of V was lowest at grid-position 1 (2.7 at. %) and increased to a maximum value at grid-position 17 (24.5 at. %). These trends were expected given the direction of precursor flow; where the Ti precursor ($TiCl_4$) entered on the left and the V precursor (VCl_4) entered on the right (Figure 2b). These trends also matched observations, where a transparent but yellow-tinged film was formed on the left (V:TiO_2) that became more dark-brown on going to the right (TiO_2: VO_2). Moving from left to right, WDX analysis demonstrated an increase in the presence of Si and a decrease in the presence of O (Figure 3). From grid-position 1 to 17 the Si level increased from 0.1 to 9.2 at. % and the O level dropped from 64.5 to 52.8

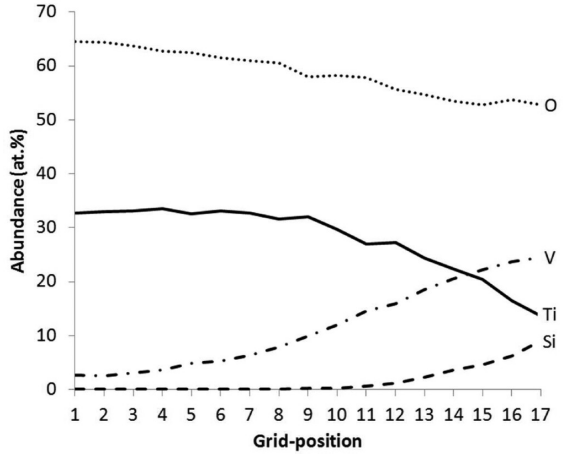

Figure 3. Chart of Ti, V, Si, and O level (at. %) determined by WDX analysis at each of the 17 grid-positions; located across a central horizontal strip of a graded TiO_2–VO_2 mixed-phase composite grown by cAPCVD.

at. %. This Si was not attributed to any Si present in the film, but rather Si from the underlying glass substrate. Therefore, the increase in Si was due to a thinner film that allowed the probe beam to better penetrate the SiO_2 substrate beneath; correlating with film thickness measurements.

X-ray Diffraction and Raman Spectroscopy. The X-ray diffraction (XRD) pattern was acquired at all 17 grid-positions (Figure 4). Two distinct phases were observed; anatase TiO_2 ($I4_1/amdz$, a = 3.785 Å, c = 9.512 Å) and monoclinic VO_2 ($P2_1/c$, a = 5.752 Å, b = 4.538 Å, c = 5.383 Å, β = 122.6°). Grid-positions 1 to 9 were found to consist primarily of the anatase TiO_2 phase. Grid-positions 10 to 14 contained a mixture of anatase TiO_2 and monoclinic VO_2. Grid-positions 15 to 17 were seemingly pure monoclinic VO_2. A change in the preferred growth of the anatase TiO_2 was observed before entering the mixed phase region (grid-positions 5 to 9), where an increase in the (200) direction [48°] was accompanied by a

dx.doi.org/10.1021/co400027p | ACS Comb. Sci. 2013, 15, 309–319

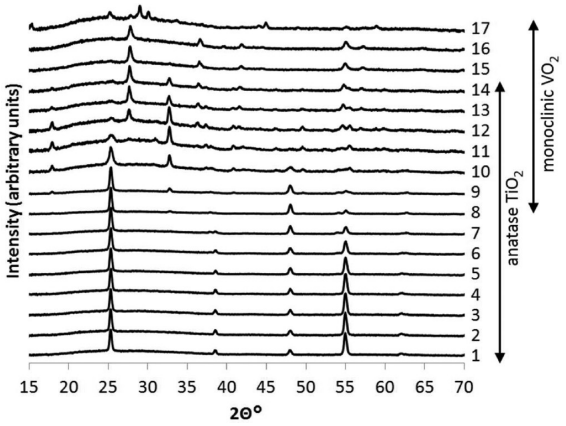

Figure 4. Stack of the X-ray diffraction patterns of all 17 grid-positions; located across a central horizontal strip of a graded TiO_2–VO_2 mixed-phase composite grown by cAPCVD.

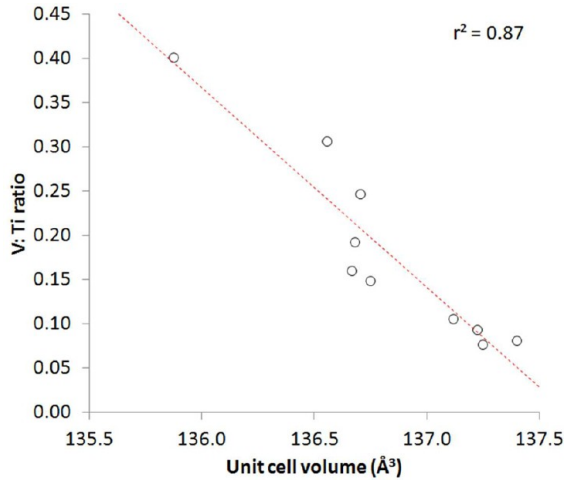

Figure 5. Plot of unit cell volume (Å^3) versus the V: Ti ratio for grid positions 1 to 10; located across a central horizontal strip of a graded TiO_2–VO_2 mixed-phase composite grown by cAPCVD.

decrease in the (105) and (211) directions [54–56°]. Stark changes in preferred growth were observed across the monoclinic VO_2 region (grid-positions 9 to 17): between grid-positions 9 to 15, preferred growth in the $(10\bar{2})$ plane was maximized [33.5°], whereas between grid-positions 11 to 17, preferred growth in the (110) plane was maximized [26.5°], and by grid-position 17, preferred growth was highest in the $(11\bar{1})$ plane [27.5°]. From grid-position 1 to 17 the intensity of XRD patterns decreased owing to an increasingly thinner and less crystalline film. Grid-positions 15 to 17 showed no observable anatase TiO_2 phase, even though interference color contours characteristic of TiO_2 were observed by eye (Figure 2a). In light of the WDX results, it was assumed amorphous TiO_2 was present in this region.

There was strong evidence for V:TiO_2 formation across grid-positions 1 to 10. This was attributed primarily to the confirmed presence of vanadium (Figure 3) alongside the yellow-tinge seen across this region, characteristic of vanadium doped TiO_2.[60] For each position in this region, the anatase TiO_2 component was fit to a Le Bail refined model. A lattice contraction was evident, with the unit cell volume decreasing from 137.4 Å^3 at grid-position 1 to 135.9 Å^3 at grid-position 10 (Table 2). Interestingly, the unit cell contracted almost linearly with an increasing presence of vanadium (Figure 5). Given the smaller size of the V^{4+} ion (0.58 Å) compared with the Ti^{4+} (0.61 Å), such a contraction was expected.

The Raman spectrum was measured at each of the 17 grid-positions. The location and phase identified by Raman spectroscopy corroborated with XRD results. Grid-positions 1 to 10 solely displayed the presence of anatase TiO_2 (Figure 6a); featuring a dominant peak at ≈150 cm^{-1} (E_g, ν_6) and less intense peaks at ≈200 (E_g, ν_5), ≈ 400 (B_{1g}, ν_4), ≈ 515 (A_{1g} and B_{1g}, ν_3 and ν_2) and ≈640 cm^{-1} (E_g, ν_1).[62] However, on moving from grid-position 1 to 10, an increasingly weak Raman pattern was obtained. This large decrease in intensity may be due to a decrease in film-crystallinity caused by phase segregation as VO_2 sites formed. The decrease in intensity continued from grid-position 11 onward. Weaker peaks were observed in this region (grid-positions 11 to 17) at 265, 400, 500, and 620 cm^{-1} and attributed to the presence of monoclinic VO_2.[63]

A general trend was observed where the width of Raman bands increased from grid-position 1 to 17. This was related to a decrease in film crystallinity across the group, as wider bands are associated with smaller crystallites. Within the anatase TiO_2 region, the center of the principal E_g vibrational mode increased from 149.3 cm^{-1} at grid-position 1 to 159.9 cm^{-1} at grid-position 10 (Figure 6b). Such a trend is typical of a lattice contraction,[64] which in this case, is caused by vanadium doping. In fact, the degree of shift resulting from the vanadium doping was almost monotonic (Figure 7) and bore a similar resemblance to the degree of unit cell contraction caused by an increasing presence of vanadium (Figure 5). It should be noted that the E_g mode in unsubstituted TiO_2 occurs at 143 cm^{-1}; this indicates that even at the far side of the film some vanadium has been introduced into the titania lattice.

For greater clarity throughout this article grid-positions will contain additional labels that represent phase and V: Ti ratio. Phases will be labeled A, A: M, and M; which mean anatase TiO_2, anatase TiO_2: monoclinic VO_2 mixtures, and monoclinic VO_2, respectively. The V: Ti ratio will be a number representative of the number of vanadium cations present per titanium cation. For example, grid-position 1 will be relabeled grid-position 1 (A–0.08). Thus meaning grid-position 1 is purely composed of the anatase TiO_2 phase and contains a vanadium doping level of 0.08 cations per titanium cation. For example, grid-position 10 will be relabeled grid-position 10 (A: M–0.40). Thus meaning grid-position 10 is composed of both the anatase TiO_2 and the monoclinic VO_2 phase and contains a vanadium presence of 0.40 cations per titanium cation.

Scanning Electron Microscopy. SEM images of the film surface were recorded for select grid-positions (Figure 8). With the exception of grid-position 9 (A–0.31), a similar grainy morphology was observed. Where other locations displayed more rounded grains, grid-position 9 (A–0.31) showed a mixture of needle-like grains and flakes. Grid-position 9 was located at the center of the film, thus separating the predominant growth of V:TiO_2 to the left and TiO_2: VO_2 composites more rich in VO_2 to the right. This more jagged morphology was attributed to the beginnings of VO_2: TiO_2 phase segregation as the solubility limit of vanadium doping in anatase TiO_2 (V: Ti ≈ 0.21)[65] was surpassed (V: Ti = 0.31). This corroborated XRD evidence that showed the beginnings of crystalline VO_2 phase formation from grid-position 8 onward (Figure 4).

Optical Properties. Reflectance and transmittance spectra were recorded over the UV–visible and near-IR range for all 17

dx.doi.org/10.1021/co400027p | ACS Comb. Sci. 2013, 15, 309–319

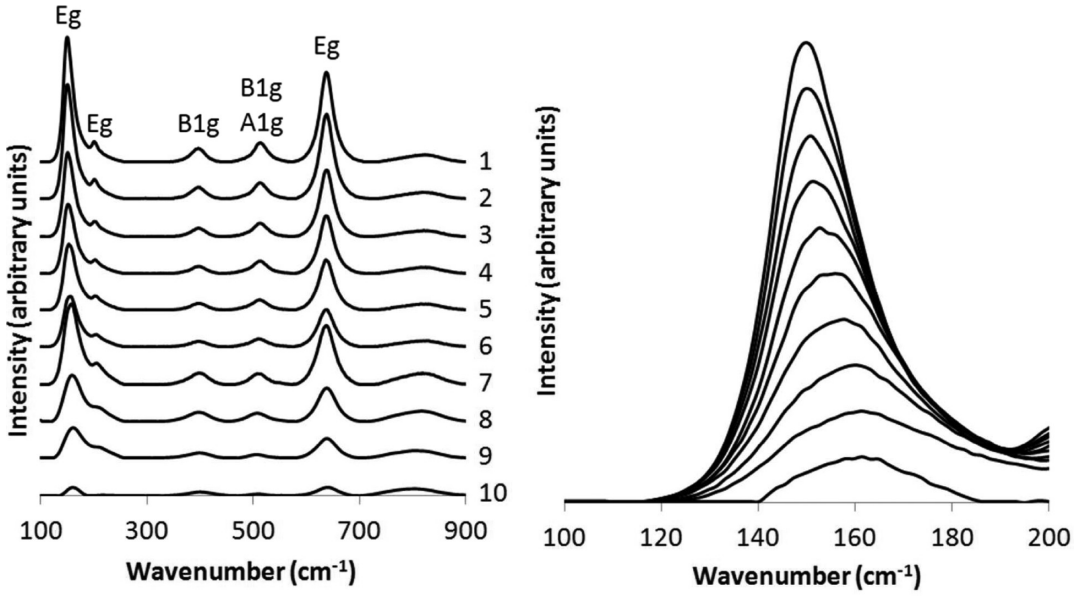

Figure 6. (a) Stack of the full Raman spectrum [anatase TiO_2 symmetry] and (b) a zoomed-in view of the principle vibrational mode [E_g, ν_6] of grid-positions 1 to 10; located across a central horizontal strip of a graded TiO_2–VO_2 mixed-phase composite grown by cAPCVD.

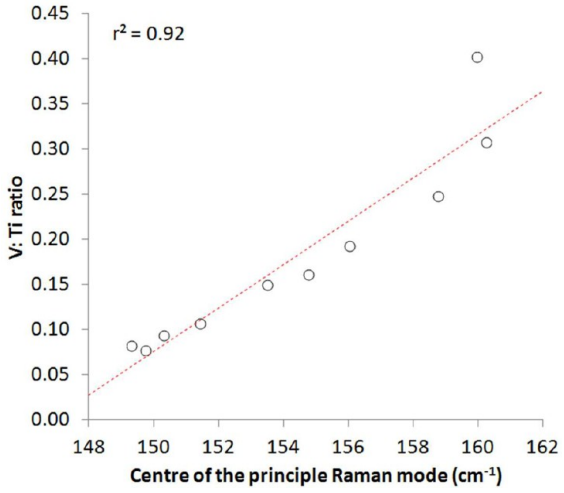

Figure 7. Plot of the central point of the principal Raman mode (cm^{-1}) versus the V: Ti ratio for grid positions 1 to 10; located across a central horizontal strip of a graded TiO_2–VO_2 mixed-phase composite grown by cAPCVD.

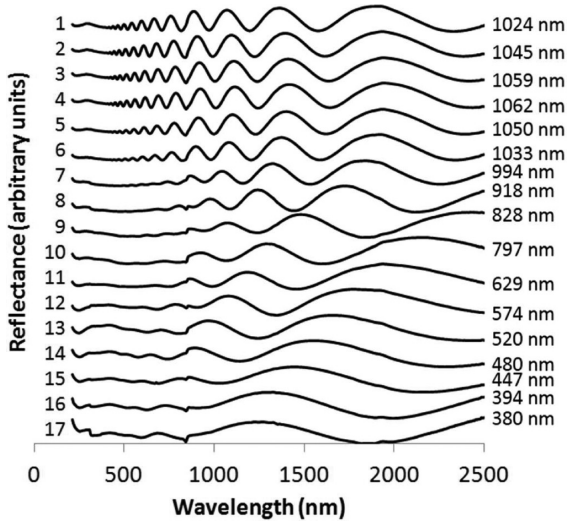

Figure 9. Stack of reflectance spectra and respective film-thickness of all 17 grid-positions; located across a central horizontal strip of a graded TiO_2–VO_2 mixed-phase composite grown by cAPCVD.

grid-positions. Both reflectance and transmittance spectra showed oscillations due to the interference of light. From these oscillations, film-thickness was determined (Table 2).[55] A stack of reflectance spectra and the calculated film-thicknesses are shown in Figure 9. A thicker film possesses a greater number of wave oscillations, as it can accommodate the constructive and destructive interference of a greater number of wavelengths. The film was thicker in the V:TiO_2 region that lay between grid-positions 1 (A–0.08) (1024 nm) and 9 (A–0.31) (828 nm). The thickest point was observed at grid-position 4

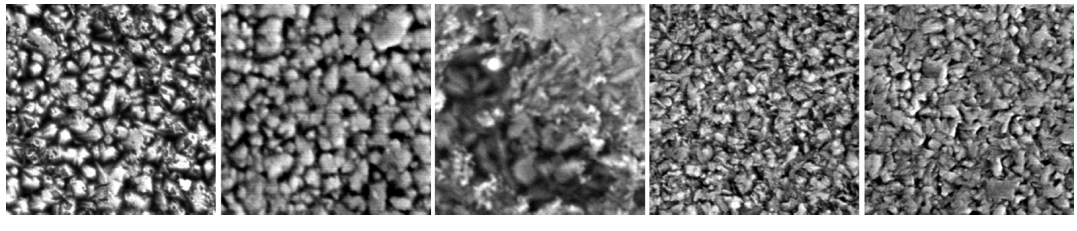

Figure 8. SEM images of the film surface for grid-positions 1, 5, 9, 13, and 17 (from left to right respectively); located across a central horizontal strip of a graded TiO_2–VO_2 mixed-phase composite grown by cAPCVD. The width of each image represents a scale of 2.4 μm.

dx.doi.org/10.1021/co400027p | ACS Comb. Sci. 2013, 15, 309–319

(A−0.11) (1062 nm). The film was significantly less thick in the mixed-phase region, decreasing in thickness from grid-position 10 (A: M−0.40) (828 nm) to 17 (M−1.81) (380 nm).

The indirect bandgap at each of the 17 grid-positions was determined from transmittance spectroscopy (Table 2). This was achieved by extrapolating Tauc plots.[54] The bandgap energy was found to decrease from 2.52 eV at grid-position 1 (A−0.08) to 0.69 eV at grid-position 17 (M−1.81). Ordinarily, undoped anatase TiO_2 shows an indirect bandgap energy of ≈3.2 eV.[38] Because of the effects of vanadium doping, a significantly reduced bandgap was observed in the region where V:TiO_2 formation was predominant (grid-positions 1 (A−0.08) to 10 (A−0.40)). In fact, a strong linear relationship existed between the level of vanadium doping and the reduced bandgap energy (Figure 10). Such a bandgap reduction in V:TiO_2 has

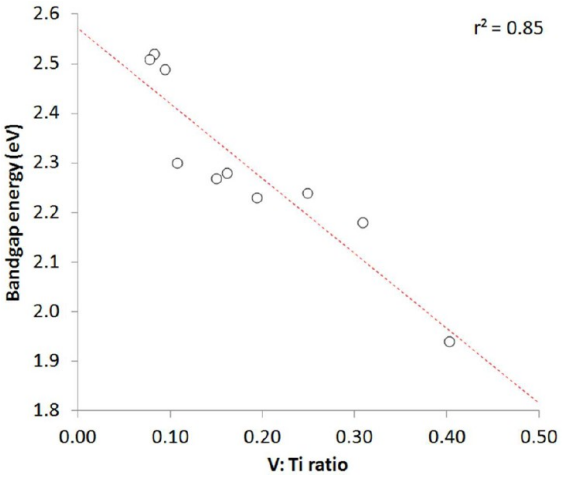

Figure 10. Plot of the indirect bandgap energy (eV) versus the V: Ti ratio for grid positions 1 to 10; located across a central horizontal strip of a graded TiO_2−VO_2 mixed-phase composite grown by cAPCVD.

been attributed to the introduction of unfilled intraband states between the valence and conduction band of TiO_2.[66] Within the mixed-phase region of the combinatorial film (grid-positions 11 (A: M−0.54) to 17 (M−1.81)) the bandgap energy decreased further. This was attributed to the increasing presence of the monoclinic VO_2 phase, which possesses a low bandgap energy of ≈0.5 eV.[67] As may be anticipated, where the highest presence of VO_2 was formed (grid-position 17 (M−1.81)), the lowest bandgap was observed (0.69 eV).

Reaction Chemistry. A graded TiO_2−VO_2 mixed-phase composite was grown from the cAPCVD reaction of $TiCl_4$ and EtAc with VCl_4 and H_2O at 550 °C. The Ti precursor ($TiCl_4$) was coupled with EtAc as the oxygen source instead of H_2O. This was because films formed from the reaction of $TiCl_4$ and H_2O are notoriously blotchy and have a tendency to flake because of the greater propensity for reactions to occur in the gas phase.[38] The exact mechanism by which $TiCl_4$ reacts with EtAc to form TiO_2 is not clear. However, it has been suggested that EtAc most probably decomposes at the surface, producing oxidant species such as ethanol, which in turn dehydrates to evolve ethane and water, invoking the hydrolysis of $TiCl_4$.[68] In contrast, the V precursor (VCl_4) could be directly coupled with H_2O, as clean and adherent films are formed because of the lower propensity for gas phase chemistry.[45]

Across the central horizontal strip analyzed, the average titanium content was 2.4 times higher than vanadium, despite the mass flow of VCl_4 (4.5×10^{-3} mol min^{-1}) being slightly higher than that of $TiCl_4$ (3.7×10^{-3} mol min^{-1}). Thus, under the conditions imposed, the reactivity of $TiCl_4$ vapor was greater than that of VCl_4 vapor.

During the combinatorial deposition, a total of 7.0 L min^{-1} of carrier gas transported the $TiCl_4$ and EtAc precursors into the reactor on the left side and 11.5 L min^{-1} of carrier transported the VCl_4 and H_2O precursors into the reactor on the right side. Given the volume of the reactor (≈ 0.25 L), these gas flows passed through the reactor in less than a second. This had a huge impact on the growth profile, inducing thickness contours to run primarily parallel to the direction of gas flow and restraining lateral diffusion. Moreover, this imposed the gradual transition in composition and phase observed, ideal for a combinatorial study.

Functional Testing. *Photoinduced Hydrophilicity.* The degree of photoinduced hydrophilicity (PIH) of all 17 grid-positions was assessed by measuring changes in the water droplet contact angle (Figure 11). Initially, contact angles

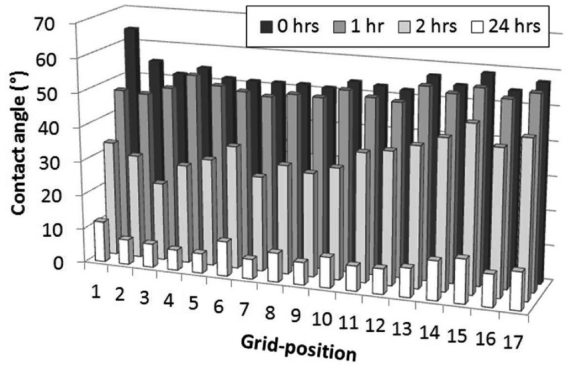

Figure 11. 3D bar chart showing the change in contact angle (deg) made by an 8.6 μL water droplet with irradiation time (254 nm, 1.74×10^{15} photons·cm^{-2} s^{-1}) at the surface of all 17 grid-positions, located across a central horizontal strip of a graded TiO_2−VO_2 mixed-phase composite grown by cAPCVD.

ranged from 50 ± 4° to 65 ± 4°, indicating a marginally hydrophilic surface. After 1 h of UVC irradiation contact angles were slightly lower (ranging from 46 ± 4° to 56 ± 4°), demonstrating a minor degree of PIH. Interestingly, those positions located within the single phase region (V:TiO_2, grid-positions 1 (A−0.08) to 9 (A−0.31) showed a greater decrease in contact angle. A further 1 h of UVC irradiation enhanced this trend, with positions located within the single phase region showing contact angles of ≈30 ± 3° and positions located within the mixed phase region showing higher contact angles that ranged from 35 ± 3° to 50 ± 4°. Notably, the decrease in contact angle was lower where more VO_2 was present. However, when irradiated for 24 h, all grid-positions showed superhydrophilic contact angles, ranging between 6 ± 1° and 13 ± 1°. It is well-known that TiO_2 can demonstrate PSH,[2] whereas monoclinic VO_2 does not possess this function. Nevertheless, this study showed that the PIH function of TiO_2 was not lost in VO_2-rich phase mixtures. However, the rate at which the superhydrophilic state was reached was hindered. This is not attributed to the reduced thickness of the film or increased amorphous nature of the TiO_2 phase in this region, as PIH is typically independent of these two properties (within the window of thicknesses herein examined).[39,40] Instead, the hindrance to the rate at which superhydrophilicity was reached

dx.doi.org/10.1021/co400027p | ACS Comb. Sci. 2013, 15, 309−319

is attributed to the lower level of TiO_2 exposed at the film-surface within the VO_2-rich region, which has a lower capacity for hydroxyl domain formation. The same effect was observed by Qureshi et al. where their 10: 90 TiO_2: VO_2 composite thin-film showed similarly hydrophilic contact angles (16 to 20°) after 12 h exposure to sunlight.[28]

Photocatalytic Activity. The photocatalytic activities of grid-position 1 (A−0.08), 5 (A−0.15), 9 (A−0.31), 13 (A: M−0.76), and 17 (M−1.81) to the UVC (254 nm, 1.74×10^{15} photons.$cm^{-2}.s^{-1}$) induced oxidation of stearic acid were assessed. The rate of stearic acid degradation was related to the decrease in IR absorption of the C−H stretches in the molecule.[58] As the flux of the light source used was known, each rate (molecules degraded·cm^{-2} s^{-1}) could be converted into a formal quantum efficiency according to eq 2, and shown in Figure 12.

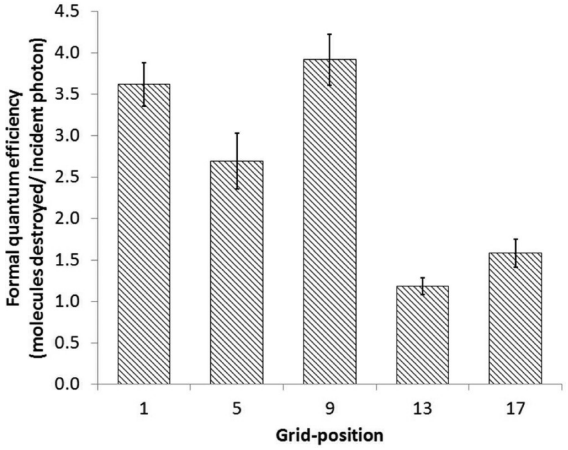

Figure 12. Bar chart of the formal quantum efficiency (FQE, molecules degraded per incident photon) from the photocatalysis of a stearic acid overlayer to 254 nm light for grid-positions 1, 5, 9, 13, and 17, located across a central horizontal strip of a graded TiO_2−VO_2 mixed-phase composite grown by cAPCVD. The width of each image represents a scale of 2.4 μm.

The highest rate of photocatalysis was found at grid-position 9 (A−0.31) (FQE = 3.92×10^{-5}). Marginally lower rates were observed at grid-positions 1 (A−0.08) (FQE = 3.62×10^{-5}) and 5 (FQE = 2.62×10^{-5}). Within the more VO_2-rich region, grid-positions 13 (A: M−0.76) (FQE = 1.18×10^{-5}) and 17 (FQE = 1.59×10^{-5}) showed rates of photocatalysis that were up to three times lower than the highest. The FQEs presented describe the molecular degradation efficiency per incident photon. However, the photo-oxidation of stearic acid is a 104 electron process;[52] therefore, the maximum FQE possible would be 9.62×10^{-3}, a case that corresponds to a photoexcitation where every incident photon photocatalytically degrades the stearic acid overlayer with 100% efficiency. Comparatively, the most photocatalytically active position in this study (grid-position 9 (A−0.31)) showed an efficiency that was 0.41% of the possible maximum.

When assessing trends in photocatalysis, variations in bandgap energy, crystallinity, surface roughness, and film-thickness must be accounted for as the activity of a photocatalyst is dependent upon these four physical properties.[38] The bandgap determines the energy at which photo-excitation can occur. As the energy of the lamp used (4.88 eV) far surpassed the bandgap of all grid-positions, variations in bandgap energy could be discounted. The variation in film-crystallinity was harder to assess since the crystal data for only grid-positions 1 (A−0.08) to 10 (A: M−0.40) could be adequately fitted to a Le Bail refined model. However, the average crystallite size was relatively constant across this region (≈ 80 nm wide). Therefore, the increase in photocatalytic activity of grid-position 9 (A−0.31) relative to grid-positions 1 (A−0.08) and 5 (A−0.15) could not be attributed to an increase in crystallinity. Additionally, film-thicknesses at grid-positions 1 (A−0.08) and 5 (A−0.15) were marginally greater (>20%) than that at grid-position 9 (A−0.31). Typically, a thicker film increases the capacity for light capture, thus enhancing photocatalysis, therefore the increased photocatalysis observed at grid-position 9 (A−0.31) relative to grid-positions 1 (A−0.08) and 5 (A−0.15) cannot be explained in terms of changes in film-thickness. Comparing the difference in surface morphology across the group (Figure 8), it is clear that grid-position 9 (A−0.31) shows the most fractured and uniquely rough topography compared to all other grid-positions analyzed. Thus, the enhancement in photocatalysis observed at grid-position 9 (A−0.31) is attributed to a more highly roughened surface that could accommodate more sites for photocatalytic processes. However, the enhancement may also have been due to a decrease in electron−hole recombination

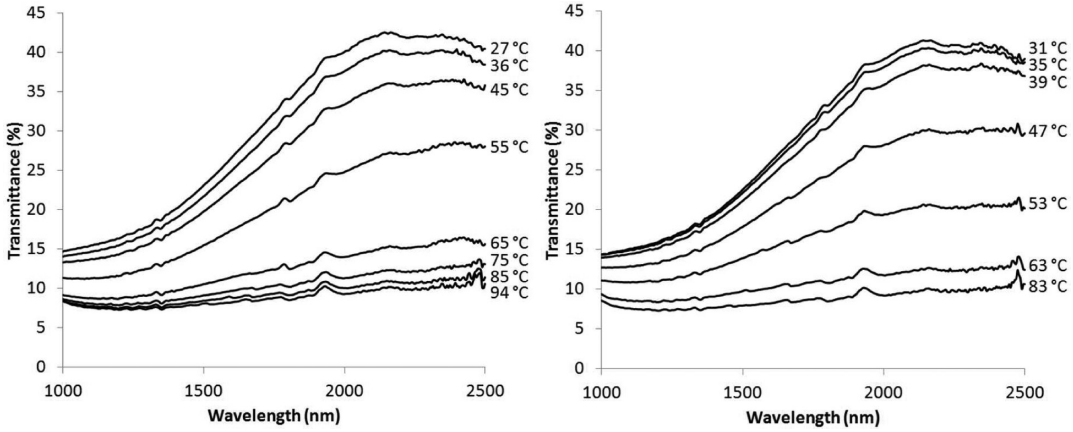

Figure 13. Change in transmittance at grid-position 17 upon (a) heating and (b) cooling; located in the most VO_2-rich region across a central horizontal strip of a graded TiO_2−VO_2 mixed-phase composite grown by cAPCVD.

dx.doi.org/10.1021/co400027p | ACS Comb. Sci. 2013, 15, 309−319

due charge transfer of photogenerated electrons in TiO_2 to VO_2 sites.

The FQEs observed in this study were low compared with pure TiO_2. For instance, P25 Degussa pellets have shown FQEs in the region of 5.0×10^{-3}, and TiO_2 thin-films have shown FQEs in the region of 2.5×10^{-3}.[11,58] Although the light source used in these experiments was about 10 times more intense, the efficiency of photocatalysis for the TiO_2 thin-films neared 2.6% of the possible maximum—an efficiency more than 6 times greater than the highest efficiency observed in this study. This is contrary to bilayered VO_2: TiO_2 films that show enhanced photocatalysis relative to pure TiO_2.[69] Thus, it is concluded that neither doping TiO_2 with vanadium nor forming a composite with VO_2 enhances UVC photocatalysis over the compositional range investigated, where a greater reduction in photocatalysis was caused by VO_2-rich composite growth. Interestingly, over the range of phase-space examined in this study, the photocatalytic activity under UVC irradiation was greatest near the solubility limit of vanadium in TiO_2, where phase segregation and composite formation begins. Previous studies have demonstrated visible light photocatalysis of V:TiO_2,[70] but in this instance when examining the V:TiO_2 region in our combinatorial system, no significant degradation of stearic acid was observed with visible light, even after a period of 1 week. However, marginal levels of visible light photocatalysis were observed within the TiO_2: VO_2 mixed-phase composite region VO_2 ($<1 \times 10^{10}$ molecules destroyed·cm^{-2} s^{-1}).

Thermochromism. Changes in the reflectance and transmittance spectra with temperature were measured in the VO_2-rich region at grid-positions 13 (A: M−0.76), 15 (M−1.09), and 17 (M−1.81). The biggest changes in transmittance and reflectance were observed between 2000 and 2500 nm in all cases. These changes were wholly reversible and attributed to the semiconductor-to-metal transition of VO_2, which typically occurs in the single crystal at 68 °C.[15] An example of the changes in IR-transmittance upon heating and cooling for grid-position 17 (M−1.81) is shown in Figure 13. A steep drop in IR-transmittance is observed upon heating from 45 to 65 °C (Figure 13a). This is attributed to the increase in free electron density with a phase change from semiconducting monoclinic VO_2 to metallic tetragonal VO_2. By 75 °C, this fall in IR-transmittance had almost reached its minimum. Upon cooling, a reverse trend was observed, with the IR-transmittance increasing to its original level and most rapidly between 63 and 39 °C (Figure 13b).

The semiconductor-to-metal transition temperature (T_C) was determined in several stages. First the transmittance/reflectance at 2000 nm was plotted against the heating/cooling temperature to form a hysteresis loop and fitted to a Boltzmann model to determine the steepest point on each slope. The steepest points were averaged, thus pin-pointing the center of each hysteresis loop, with the center being defined as T_C. This yielded a T_C from changes in transmittance and a T_C from changes in reflectance. These two values were averaged to give an overall T_C value for the material, the error being defined as half the range (Table 2). From grid-position 13 (A: M−0.76) to 15 (M−1.09) the T_C fell from 56.2 ± 0.7 °C to 50.5 ± 4.7 °C. However, moving from grid-position 15 (M−1.09) to 17 (M−1.81) there was no significant change in T_C, with a T_C of 50.6 ± 1.3 °C observed at grid-position 17 (M−1.81). In each case there was a reduction in T_C relative to pure VO_2.[15] Similar reductions in T_C were observed by both Qureshi et al. in their mixed phase TiO_2: VO_2 composite (54 °C)[28] and by Sheel et al. in their VO_2: TiO_2 bilayer (55 °C),[69] both of whom used an APCVD system and attributed these reductions to film-strain. Such strain may well have been present in this system, induced by the minor levels of amorphous V:TiO_2 dispersed throughout the VO_2-rich region.

IV. CONCLUSION

A combinatorial film with a phase gradient from V:TiO_2 (V: Ti ≥ 0.08), through a range of TiO_2−VO_2 composites, to a vanadium-rich composite (V: Ti = 1.81) was grown by combinatorial atmospheric pressure chemical vapor deposition (cAPCVD). The film was grown from the reaction of $TiCl_4$, VCl_4, ethyl acetate (EtAc), and H_2O at 550 °C on glass. The gradient in gas mixtures across the reactor induced compositional film growth, producing a single film with many phases and compositions at different positions. Seventeen unique positions distributed evenly along a central horizontal strip were investigated. Comparison of the physical and functional properties across this system enabled a number of key findings to be established:

1. When the solubility limit of vanadium in TiO_2 was reached a composite material was formed containing both VO_2 and V:TiO_2 phases.
2. This combinatorial study of vanadium doping a TiO_2 thin-film is the first of its kind, demonstrating solid solution formation up to the solubility limit. This was shown by the shift in the E_g Raman band, contraction in the anatase unit cell, and reduction in the bandgap energy with good correlation versus vanadium content (r^2 = 0.87−0.92).
3. The rate of film growth was considerably faster for $TiCl_4$ than VCl_4 in this system despite being introduced at a lower molar flow and with a less potent oxygen source (ethyl acetate versus water).
4. The combinatorial approach enabled the formation of a region of the film that simultaneously displayed four functional properties: photoinduced hydrophilicity, photocatalysis, a reduced bandgap, and a reduced thermochromic transition temperature.
5. The rate of photoinduced hydrophilicity was inhibited by an increasing presence of VO_2, but it was still possible to generate a superhydrophilic state after a sustained period of illumination, even within a highly VO_2-rich composite (V: Ti = 1.81).
6. A maximum level of UVC photocatalysis was observed at a position bordering the solubility limit of V:TiO_2 (V: Ti ≈ 0.21) and fragmentation into a mixed-phase composite. This is attributed to an enhanced surface roughness, but may also be due to a decrease in electron−hole recombination because of the charge transfer of photogenerated electrons from TiO_2 to VO_2 sites. However, rates of UVC photocatalysis were typically lower than films containing pure TiO_2.
7. A decrease in the semiconductor-to-metal transition temperature (T_C) of up to 18 °C was observed within the mixed-phase TiO_2: VO_2 composite region (V: Ti = 1.09 to 1.81). This is attributed to an increase in film strain caused by the surrounding V:TiO_2 phase. It is possible that some Ti could have entered the VO_2 lattice and caused the reduction in T_C; however this was not observed in the XRD patterns as no real change in unit cell size was discerned compared to a VO_2 standard, unlike the TiO_2 portion of the film.

Analyzing combinatorial thin-film systems provides a shortcut to understanding physical-functional property relationships

dx.doi.org/10.1021/co400027p | ACS Comb. Sci. 2013, 15, 309−319

and provides a faster way of discovering new materials and optimizing composition.

■ ASSOCIATED CONTENT

Supporting Information

The emission profile of the UVC lamp used in this study (Figure S1). This material is available free of charge via the Internet at http://pubs.acs.org.

■ AUTHOR INFORMATION

Corresponding Author

*E-mail: i.p.parkin@ucl.ac.uk. Phone: +44 (0)20 7679 4669. Fax: +44 (0)20 7679 7463.

Author Contributions

The manuscript was written through contributions of all authors. All authors have given approval to the final version of the manuscript.

Funding

I.P.P. and C.J.C. would like to thank the EPSRC for funding (platform grant EP/H00064X) and Pilkington for the glass. A.K. would like to thank the Ramsay Memorial Fellowships Trust for funding. The authors gratefully acknowledge the Deanship of Scientific Research (DSR), King Abdulaziz University, their technical and financial support (Grant D-5/432).

Notes

The authors declare no competing financial interest.

■ ABBREVIATIONS

APCVD, atmospheric pressure chemical vapor deposition; EtAc, ethyl acetate; WDX, wavelength dispersive X-ray; XRD, X-ray diffraction; SEM, scanning electron microscopy; PIH, photoinduced hydrophilicity; UVC, ultraviolet between 100 and 280 nm; T_C, semiconductor-to-metal transition; PVD, physical vapor deposition; cAPCVD, combinatorial atmospheric pressure chemical vapor deposition; CCD, charge-coupled device; FT-IR, Fourier transform-infrared; at. %, atomic %

■ REFERENCES

(1) Mills, A.; Le Hunte, S. An overview of semiconductor photocatalysis. *J. Photochem. Photobiol., A* **1997**, *108*, 1.

(2) Fujishima, A.; Zhang, X.; Tryk, D. TiO2 photocatalysis and related surface phenomena. *Surf. Sci. Rep.* **2008**, *63*, 515.

(3) Selli, E.; Chiarello, G. L.; Quartarone, E.; Mustarelli, P.; Rossetti, I.; Forni, L. A photocatalytic water splitting device for separate hydrogen and oxygen evolution. *Chem. Commun.* **2007**, *1*, 5022.

(4) Mills, A.; Valenzuela, M. The photo-oxidation of water by sodium persulfate, and other electron acceptors, sensitised by TiO2. *J. Photochem. Photobiol., A* **2004**, *165*, 25.

(5) Osterloh, F. E. Inorganic Materials as Catalysts for Photochemical Splitting of Water. *Chem. Mater.* **2008**, *20*, 35.

(6) Savage, N. Composite n−p semiconducting titanium oxides as gas sensors. *Sens. Actuators, B* **2001**, *79*, 17.

(7) Dunnill, C. W.; Aiken, Z. A.; Pratten, J.; Wilson, M.; Morgan, D. J.; Parkin, I. P. Enhanced photocatalytic activity under visible light in N-doped TiO2 thin films produced by APCVD preparations using t-butylamine as a nitrogen source and their potential for antibacterial films. *J. Photochem. Photobiol., A* **2009**, *207*, 244.

(8) Page, K.; Palgrave, R. G.; Parkin, I. P.; Wilson, M.; Savin, S. L. P.; Chadwick, A. V. Titania and silver/titania composite films on glass; potent antimicrobial coatings. *J. Mater. Chem.* **2007**, *17*, 95.

(9) Rampaul, A.; Parkin, I. P.; O'Neill, S. A.; Desouza, J.; Mills, A.; Elliott, N. Titania and tungsten doped titania thin films on glass; active photocatalysts. *Polyhedron* **2003**, *22*, 35.

(10) Dunnill, C. W.; Aiken, Z. A.; Kafizas, A.; Pratten, J.; Wilson, M.; Morgan, D. J.; Parkin, I. P. White light induced photocatalytic activity of sulfur-doped TiO2 thin films and their potential for antibacterial application. *J. Mater. Chem.* **2009**, *19*, 8747.

(11) Kafizas, A.; Kellici, S.; Darr, J. A.; Parkin, I. P. Titanium dioxide and composite metal/metal oxide titania thin films on glass: A comparative study of photocatalytic activity. *J. Photochem. Photobiol., A* **2009**, *204*, 183.

(12) Binions, R.; Piccirillo, C.; Palgrave, R. G.; Parkin, I. P. Hybrid Aerosol Assisted and Atmospheric Pressure CVD of Gold-Doped Vanadium Dioxide. *Chem. Vap. Deposition* **2008**, *14*, 33.

(13) Blackman, C. S.; Piccirillo, C.; Binions, R.; Parkin, I. P. Atmospheric pressure chemical vapour deposition of thermochromic tungsten doped vanadium dioxide thin films for use in architectural glazing. *Thin Solid Films* **2009**, *517*, 4565.

(14) Manning, T. D.; Parkin, I. P.; Pemble, M. E.; Sheel, D.; Vernardou, D. Intelligent Window Coatings: Atmospheric Pressure Chemical Vapor Deposition of Tungsten-Doped Vanadium Dioxide. *Chem. Mater.* **2004**, *16*, 744.

(15) Manning, T. D.; Parkin, I. P.; Blackman, C. S.; Qureshi, U. APCVD of thermochromic vanadium dioxide thin films−solid solutions V2−xMxO2 (M = Mo, Nb) or composites VO2 - SnO2.pdf. *J. Mater. Chem.* **2005**, *15*, 4560.

(16) Binions, R.; Hyett, G.; Piccirillo, C.; Parkin, I. P. Doped and un-doped vanadium dioxide thin films prepared by atmospheric pressure chemical vapour deposition from vanadyl acetylacetonate and tungsten hexachloride: the effects of thickness and crystallographic orientation on thermochromic properties. *J. Mater. Chem.* **2007**, *17*, 4652.

(17) Piccirillo, C.; Binions, R.; Parkin, I. P. Synthesis and Functional Properties of Vanadium Oxides: V2O3, VO2, and V2O5 Deposited on Glass by Aerosol-Assisted CVD. *Chem. Vap. Deposition* **2007**, *13*, 145.

(18) Kanu, S. S.; Binions, R. Thin films for solar control applications. *Proc. R. Soc., A* **2009**, *466*, 19.

(19) Binions, R.; Piccirillo, C.; Parkin, I. P. Tungsten doped vanadium dioxide thin films prepared by atmospheric pressure chemical vapour deposition from vanadyl acetylacetonate and tungsten hexachloride. *Surf. Coat. Technol.* **2007**, *201*, 9369.

(20) Manning, T. D.; Parkin, I. P. Vanadium(IV) oxide thin films on glass and silicon from the atmospheric pressure chemical vapour deposition reaction of VOCl3 and water. *Polyhedron* **2004**, *23*, 3087.

(21) Morin, F. Oxides Which Show a Metal-to-Insulator Transition at the Neel Temperature. *Phys. Rev. Lett.* **1959**, *3*, 34.

(22) O'Neill, S. A.; Clark, R. J. H.; Parkin, I. P.; Elliott, N.; Mills, A. Anatase Thin Films on Glass from the Chemical Vapor Deposition of Titanium(IV) Chloride and Ethyl Acetate. *Chem. Mater.* **2003**, *15*, 46.

(23) Kafizas, A.; Dunnill, C. W.; Parkin, I. P. The relationship between photocatalytic activity and photochromic state of nano-particulate silver surface loaded titanium dioxide thin-films. *Phys. Chem. Chem. Phys.* **2011**, *13*, 13827.

(24) Partlow, D. P.; Gurkovich, S. R.; Radford, K. C.; Denes, L. J. Switchable vanadium oxide films by a sol-gel process. *J. Appl. Phys.* **1991**, *70*, 443.

(25) Martin, N.; Rousselot, C.; Rondot, D.; Palmino, F.; Mercier, R. Microstructure modification of amorphous titanium oxide thin films during annealing treatment. *Thin Solid Films* **1997**, *300*, 113−121.

(26) Lee, M.-H.; Kim, M.-G. RTA and stoichiometry effect on the thermochromism of VO2 thin films. *Thin Solid Films* **1996**, *286*, 219−222.

(27) Kafizas, A.; Parkin, I. P. *Materials for a Sustainable Future*, 1st ed.; Letcher, T. M., Scott, J. L., Eds.; The Royal Society of Chemistry: Cambridge, U.K., 2012; Chapter 20 - Glass and New Technologies, pp 644−667.

(28) Qureshi, U.; Manning, T. D.; Blackman, C.; Parkin, I. P. Composite thermochromic thin films: (TiO2)−(VO2) prepared from titanium isopropoxide, VOCl3 and water. *Polyhedron* **2006**, *25*, 334.

(29) Qureshi, U.; Manning, T. D.; Parkin, I. P. Atmospheric pressure chemical vapour deposition of VO2 and VO2/TiO2 films from the reaction of VOCl3, TiCl4 and water. *J. Mater. Chem.* **2004**, *14*, 1190.

(30) Kafizas, A.; Parkin, I. P. Inorganic thin-film combinatorial studies for rapidly optimizing functional properties. *Chem. Soc. Rev.* **2012**, *41*, 738.
(31) Chang, K.-S.; Green, M. L.; Suehle, J.; Vogel, E. M.; Xiong, H.; Hattrick-Simpers, J.; Takeuchi, I.; Famodu, O.; Ohmori, K.; Ahmet, P.; Chikyow, T.; Majhi, P.; Lee, B.-H.; Gardner, M. Combinatorial study of Ni−Ti−Pt ternary metal gate electrodes on HfO[sub 2] for the advanced gate stack. *Appl. Phys. Lett.* **2006**, *89*, 142108.
(32) Cui, J.; Chu, Y. S.; Famodu, O. O.; Furuya, Y.; Hattrick-Simpers, J.; James, R. D.; Ludwig, A.; Thienhaus, S.; Wuttig, M.; Zhang, Z.; Takeuchi, I. Combinatorial search of thermoelastic shape-memory alloys with extremely small hysteresis width. *Nat. Mater.* **2006**, *5*, 286.
(33) Matsumoto, Y.; Murakami, M.; Shono, T.; Hasegawa, T.; Fukumura, T.; Kawasaki, M.; Ahmet, P.; Chikyow, T.; Koshihara, S.; Koinuma, H. Room-Temperature Ferromagnetism in Transparent Transition Metal-Doped Titanium Dioxide. *Science* **2001**, *291*, 854.
(34) Wang, J.; Yoo, Y.; Gao, C.; Takeuchi, I.; Sun, X.; Chang, H.; Xiang, X.-D.; Schultz, P. G. Identification of a Blue Photoluminescent Composite Material from a Combinatorial Library. *Science* **1998**, *279*, 1712.
(35) Hyett, G.; Green, M.; Parkin, I. P. An Investigation of Titanium-Vanadium Nitride Phase Space, Conducted Using Combinatorial Atmospheric Pressure CVD. *Chem. Vap. Deposition* **2008**, *14*, 309.
(36) Hyett, G.; Parkin, I. P. A combinatorial approach to phase synthesis and characterisation in atmospheric pressure chemical vapour deposition. *Surf. Coat. Technol.* **2007**, *201*, 8966.
(37) Hyett, G.; Green, M.; Parkin, I. P. The use of combinatorial chemical vapor deposition in the synthesis of Ti(3-delta)O4N with 0.06 < delta < 0.25: a titanium oxynitride phase isostructural to anosovite. *J. Am. Chem. Soc.* **2007**, *129*, 15541.
(38) Kafizas, A.; Carmalt, C. J.; Parkin, I. P. Does a Photocatalytic Synergy in an Anatase-Rutile TiO2 Composite Thin-Film Exist? *Chem.—Eur. J.* **2012**, *18*, 13048.
(39) Kafizas, A.; Parkin, I. P. Combinatorial atmospheric pressure chemical vapor deposition (cAPCVD): a route to functional property optimization. *J. Am. Chem. Soc.* **2011**, *133*, 20458.
(40) Kafizas, A.; Dunnill, C. W.; Parkin, I. P. Combinatorial atmospheric pressure chemical vapour deposition (cAPCVD) of niobium doped anatase; effect of niobium on the conductivity and photocatalytic activity. *J. Mater. Chem.* **2010**, *20*, 8336.
(41) Kafizas, A.; Parkin, I. P. The combinatorial atmospheric pressure chemical vapour deposition (cAPCVD) of a gradating N-doped mixed phase titania thin film. *J. Mater. Chem.* **2010**, *20*, 2157.
(42) Kafizas, A.; Dunnill, C. W.; Hyett, G.; Parkin, I. P. Combinatorial CVD: New Oxynitride Photocatalysts. *ECS Trans.* **2010**, *25*, 139.
(43) Hyett, G.; Green, M.; Parkin, I. P. X-ray diffraction area mapping of preferred orientation and phase change in TiO2 thin films deposited by chemical vapor deposition. *J. Am. Chem. Soc.* **2006**, *128*, 12147.
(44) Kafizas, A.; Crick, C.; Parkin, I. P. The combinatorial atmospheric pressure chemical vapour deposition (cAPCVD) of a gradating substitutional/interstitial N-doped anatase TiO2 thin-film; UVA and visible light photocatalytic activities. *J. Photochem. Photobiol., A* **2010**, *216*, 156.
(45) Kafizas, A.; Hyett, G.; Parkin, I. P. Combinatorial atmospheric pressure chemical vapour deposition (cAPCVD) of a mixed vanadium oxide and vanadium oxynitride thin film. *J. Mater. Chem.* **2009**, *19*, 1399.
(46) Kim, K. W.; Jeon, M. K.; Oh, K. S.; Kim, T. S.; Kim, Y. S.; Woo, S. I. Combinatorial approach for ferroelectric material libraries prepared by liquid source misted chemical deposition method. *Proc. Natl. Acad. Sci. U.S.A.* **2007**, *104*, 1134.
(47) Smith, R. C.; Hoilien, N.; Roberts, J. T.; Campbell, S. A.; Gladfelter, W. L. Combinatorial chemical vapor deposition of metal dioxides using anhydrous metal nitrates (CVD - di-electrics). *Chem. Mater.* **2002**, *14*, 474.
(48) Xia, B.; Chen, F.; Campbell, S. A.; Roberts, J. T.; Gladfelter, W. L. Combinatorial CVD of Zirconium, Hafnium, and Tin Oxide Mixtures for Applications as High-κ Materials. *Chem. Vap. Deposition* **2004**, *10*, 195.
(49) Zhong, L.; Zhang, Z.; Campbell, S. A.; Gladfelter, W. L. Combinatorial CVD of ZrO2 or HfO2 compositional spreads with SiO2 for high K dielectrics. *J. Mater. Chem.* **2004**, *14*, 3203.
(50) Kuykendall, T.; Ulrich, P.; Aloni, S.; Yang, P. Complete composition tunability of InGaN nanowires using a combinatorial approach. *Nat. Mater.* **2007**, *6*, 951.
(51) Kafizas, A.; Adriaens, D.; Mills, A.; Parkin, I. P. Simple method for the rapid simultaneous screening of photocatalytic activity over multiple positions of self-cleaning films. *Phys. Chem. Chem. Phys.* **2009**, *11*, 8367.
(52) Kafizas, A.; Mills, A.; Parkin, I. P. A comprehensive aerosol spray method for the rapid photocatalytic grid area analysis of semiconductor photocatalyst thin films. *Anal. Chim. Acta* **2010**, *663*, 69.
(53) Betsch, R. J. Parametric analysis of control parameters in MOCVD. *J. Cryst. Growth* **1986**, *77*, 210.
(54) Tauc, J. Optical properties and electronic structure of amorphous Ge and Si. *Mater. Res. Bull.* **1968**, *3*, 37.
(55) Swanepoel, R. J. Determination of the thickness and optical constants of amorphous silicon. *J. Phys. E: Sci. Instrum.* **1983**, *16*, 1214.
(56) Tu, R.; Goto, T. High Temperature Stability of Anatase Films Prepared by MOCVD. *Mater. Trans.* **2008**, *49*, 2040.
(57) Kana Kana, J. B.; Ndjaka, J. M.; Vignaud, G.; Gibaud, A.; Maaza, M. Thermally tunable optical constants of vanadium dioxide thin films measured by spectroscopic ellipsometry. *Opt. Commun.* **2011**, *284*, 807.
(58) Mills, A.; Wang, J. Simultaneous monitoring of the destruction of stearic acid and generation of carbon dioxide by self-cleaning semiconductor photocatalytic films. *J. Photochem. Photobiol., A* **2006**, *182*, 181.
(59) *Origin 8.0*; OriginLab: Northhampton, MA, 2009.
(60) Bettinelli, M.; Dallacasa, V.; Falcomer, D.; Fornasiero, P.; Gombac, V.; Montini, T.; Romanò, L.; Speghini, A. Photocatalytic activity of TiO2 doped with boron and vanadium. *J. Hazard. Mater.* **2007**, *146*, 529.
(61) Chalker, P. R.; Bull, S. J.; Rickerby, D. S. A review of the methods for the evaluation of coating-substrate adhesion. *Mater. Sci. Eng.: A* **1991**, *140*, 583.
(62) Ohsaka, T.; Izumi, F.; Fujiki, Y. Raman spectrum of anatase, TiO2. *J. Raman Spectrosc.* **1978**, *7*, 321.
(63) Wei, J.; Ji, H.; Guo, W.; Nevidomskyy, A. H.; Natelson, D. Hydrogen stabilization of metallic vanadium dioxide in single-crystal nanobeams. *Nat. Nanotechnol.* **2012**, *7*, 357.
(64) Harunsani, M. H.; Oropeza, F. E.; Palgrave, R. G.; Egdell, R. G. Electronic and Structural Properties of Sn x Ti 1− x O 2 ($0.0 \leq x \leq 0.1$) Solid Solutions. *Chem. Mater.* **2010**, *22*, 1551.
(65) Le Roy, D.; Valloppilly, S.; Skomski, R.; Liou, S.-H.; Sellmyer, D. J. Magnetism and structure of anatase (Ti1−xVx)O2 films. *J. Appl. Phys.* **2012**, *111*, 07C118.
(66) Zhang, H.; Chen, G.; Bahnemann, D. W. Photoelectrocatalytic materials for environmental applications. *J. Mater. Chem.* **2009**, *19*, 5089.
(67) Yin, W.; Wolf, S.; Ko, C.; Ramanathan, S.; Reinke, P. Nanoscale probing of electronic band gap and topography of VO[sub 2] thin film surfaces by scanning tunneling microscopy. *J. Appl. Phys.* **2011**, *109*, 024311.
(68) Evans, P.; Pemble, M. E.; Sheel, D. W. Precursor-Directed Control of Crystalline Type in Atmospheric Pressure CVD Growth of TiO2 on Stainless Steel. *Chem. Mater.* **2006**, *18*, 5750.
(69) Evans, P.; Pemble, M. E.; Sheel, D. W.; Yates, H. M. Multifunctional self-cleaning thermochromic films by atmospheric pressure chemical vapour deposition. *J. Photochem. Photobiol., A* **2007**, *189*, 387.
(70) Gu, D.-E.; Yang, B.-C.; Hu, Y.-D. A Novel Method for Preparing V-doped Titanium Dioxide Thin Film Photocatalysts with High Photocatalytic Activity Under Visible Light Irradiation. *Catal. Lett.* **2007**, *118*, 254.